Journal of Physics and Chemistry of Solids 75 (2014) 366–373

Contents lists available at ScienceDirect

Journal of Physics and Chemistry of Solids

journal homepage: www.elsevier.com/locate/jpcs

Study of Kβ X-ray emission spectroscopy applied to $Mn_{(2-x)}V_{(1+x)}O_4$ ($x=0$ and 1/3) oxyspinel and comparison with XANES

S. Ceppi [a], A. Mesquita [b], F. Pomiro [c], E.V. Pannunzio Miner [c], G. Tirao [a,*]

[a] IFEG-CONICET and Facultad de Matemática, Astronomía y Física, Universidad Nacional de Córdoba, Ciudad Universitaria, 5000 Córdoba, Argentina
[b] Instituto de Geociências e Ciências Exatas, Universidade Estadual Paulista, 13506-900 Rio Claro, São Pablo, Brazil
[c] INFIQC-CONICET and Departamento de Fisicoquímica, Facultad de Ciencias Químicas, Universidad Nacional de Córdoba, Ciudad Universitaria, 5000 Córdoba, Argentina

ARTICLE INFO

Article history:
Received 23 April 2013
Received in revised form
11 October 2013
Accepted 7 November 2013
Available online 15 November 2013

Keywords:
A. Oxides
C. XAFS

ABSTRACT

Oxidation state and coordination of transition metal cations seems to be hard to assess when considering multiple cations, each one with different possible oxidation states. In fact, this is the case of the spinel-type double oxides family. High resolution Kβ X-ray fluorescence spectra were measured in $Mn_{(2-x)}V_{(1+x)}O_4$ ($x=0$ and $\frac{1}{3}$) spinels-type double oxides in order to determine the oxidation state and coordination of V and Mn cations. The relative intensity of radiative Auger effect $KM_{2,3}M_{4,5}$ to the total intensity and the integral absolute difference value were used as reference parameters for the characterization of Mn oxidation states. The coordination of Mn ions was inferred by the intensity of the $K\beta_5$ line. In the case of V compounds, it was used as the intensity of the line $K\beta'$ relative to the total area of Kβ region. The obtained results were further compared with X-ray absorption spectra analysis, showing good agreements regarding the oxidation state characterization. However, there were found some discrepancies in coordination, due to customary oversimplifications in the $K\beta_5$ line origin. The obtained results might represent valuable and useful data for chemical scopes of characterizing spinel-type oxides family.

1. Introduction

The characterization of the oxidation state and occupation sites is a challenge typically found when studying and developing new materials since magnetic and electrical properties may be determined. Moreover, it is possible to take advantage from this characterization method for appropriate description, control and prediction of materials physical properties. Particularly, the spinel-type oxides are interesting and promising materials due to potential technological applications. Actually, they are widely studied mainly motivated by diverse effects arising from different electronic correlations related to chemical composition and crystal structure. Spinel-type compounds [1–3] are considered as new research topic in the field of materials science since the discovery of the magnetoresistance effect [4]. Spinel-type oxides exhibit AB_2O_4 stoichiometry, where A and B are cations of either 2+ and 3+ charge or of 4+ and 2+ charge. This kind of materials present structures described as a densely packed oxygen array with A and B cations in tetrahedral (T) and octahedral (O) coordination, respectively. A precise knowledge about cation distribution is useful and sometimes mandatory for attaining improved understanding of the physical and magnetic properties, it is necessary to determine the oxidation states and distribution between T and O sites of Mn and V.

There are many techniques that can be used to study the cations oxidation state and distribution between T and O sites. Customary X-ray absorption fine structure (XAFS) [5] is the technique most commonly used to explore low concentrated metals or poor crystalline systems, e.g., to study the Mn coordination in doped perovskite $SrTiO_3$ [6]. X-ray diffraction anomalous fine structure is also used to obtain element-specific and site-specific information on site occupancy, local structure, and valency in epitaxial manganese ferrite thin films [7]. Okita et al. [8] employed the X-Ray Anomalous Scattering to determine the cation distribution in Mn–Zn–Fe ferrite, and Eba and Sakurai [2] reported successful determination for manganese spinels by analyzing Kβ X-ray fluorescence spectra investigating in detail ratio of intensities between $K\beta'$ satellite and $K\beta_5$ bands. Although it is known that there are also other conventional techniques for studying the chemical environment of this type of metals, it is remarkable that the obtained results were highly satisfactory, due to the high reliability of the determination of the oxidation states.

In this paper, a detailed study of high resolution Kβ X-ray emission spectra of family members spinel $Mn_{(2-x)}V_{(1+x)}O_4$ ($x=0$

* Corresponding author. Tel.: +54 351 4334051; fax: +54 351 4334054.
E-mail address: gtirao@famaf.unc.edu.ar (G. Tirao).

0022-3697/$ - see front matter © 2013 Elsevier Ltd. All rights reserved.
http://dx.doi.org/10.1016/j.jpcs.2013.11.002

and $\frac{1}{3}$) was performed in order to determine the oxidation states and the coordination. Synthetic standards were used with known oxidation states of Mn and V for further comparisons with studied samples. For analysis purposes different spectral parameters were used as reference. The relative intensities between RAE $KM_{2,3}M_{4,5}$ to the total Kβ region, and the integral of the absolute values of the difference between two spectra and the $K\beta_5$ relative intensity were used for Mn characterizations. In the case of V compounds, the reference spectral parameter was the intensity of the line Kβ′ relative to the total area was used. The results were contrasted with X-ray absorption spectra analysis, obtaining very good agreements, which might suggest a validation of the X-ray emission spectroscopy as a powerful technique for studying chemical environment.

2. Theoretical background

2.1. Kβ X-ray emission spectroscopy

High resolution X-ray emission spectroscopy (XES) experiments are based on measuring changes in some spectral features in correspondence to specific chemical environment. Different X-ray spectra properties may be modified like X-ray energy shifts, satellite lines (if any) and variation of line shapes and relative intensities. Electronic transitions from the molecular orbitals to a core-level are suitable candidates for chemically sensitive fluorescence lines, since the character of the molecular orbitals depends on the specific chemical species, thus the effect on the structure of the emission spectrum may be clearly observed [9]. Electron changes $3p \rightarrow 1s$ in transition metal compounds represent the main contribution the Kβ X-ray emission spectra and thereby the $K\beta_{1,3}$ line is dominant; whereas satellite structures might provide information about oxidation state, ligand type and metal–ligand bonding length [9–15]. The main Kβ region splits into multiplets spread over a region of about 15 eV, being mainly composed of the strong $K\beta_{1,3}$ line and a less intense Kβ′ and $K\beta_x$ satellite lines at lower energies. These structures may be explained by ligand field multiplet model [16], where Kβ′ line is due to the 3p3d exchange interaction and $K\beta_x$ line due to spin flip of the 3d electron.

Besides the radiative events, the reorganization of an atom might be due to radiative Auger transitions. The Radiative Auger Effect (RAE) causes a satellite structure on the low energy side of the main peak [17]. The RAE is a process competitive to emission of the diagram line, in which the inner-shell hole is filled by a transition of an electron from an outer shell electron. This process results in photon emission simultaneously with an outer shell electron transition to an unoccupied atomic bound state or the continuum. Then, the emitted X-ray photon shares its energy with the excited electron. The KM_iM_j represents a $K \rightarrow M_i$ transition where the relaxation energy is sheared with a photon of energy $h\nu$ and an Auger electron ejected from the M_j shell with a kinetic energy E_{el} [18,19]. In the particular case of $i=2,3$ and $j=4,5$ ($KM_{2,3}M_{4,5}$) the RAE transitions correspond to $K \rightarrow M_{2,3}$ transitions that could be associated to the $K\beta_{1,3}$ line with emission of an $M_{4,5}$ electron with a bounding energy $E(M_{4,5})=3.3 \pm 0.5$ eV for Mn atoms [20]. Therefore, the emitted photon energy is $h\nu = E(K\beta_{1,3}) - E(M_{4,5}) - E_{el}$, according to energy conservation. This phenomenon is observed as a peak located at the low-energy side of peak $K\beta_{1,3}$ main peak producing an asymmetric peak shape. For first row transition atoms, variations in the $KM_{2,3}M_{4,5}$ RAE intensity is related with the oxidation state, since this line is related to 3d electrons. Actually, it was studied for different Ti [19] and Fe compounds [21,22].

At energies higher than those corresponding to $K\beta_{1,3}$ line, two structures of lines Kβ″ and $K\beta_5$ are observed that may be interpreted by the MO theory [23]. The Kβ″ line is originated from transitions of molecular orbital, $4t_2 \rightarrow 1a_1$ ($4t_{1u} \rightarrow 1a_1$) transition for T (O) symmetry, with mainly contribution of ligand-2s, to the atomic orbital 1s of the central atom [24]. On the other hand, the $K\beta_5$ band is formed by transitions filling the metal 1s vacancy from molecular orbitals with mainly atomic orbital contributions of ligand-2p and metal-3d (ligand-2p) for T (O) symmetry [24].Then, the $K\beta_5$ band involves a valence-to-core transitions which are chemically sensitive and can be used to study the chemical environment [10–13].

The sensitivity to chemical environment, along with the strong correlation between experiment and theory, suggests that the high-resolution Kβ emission spectra might be a useful predictive tool for atom active site characterization. Kβ-XES techniques were previously successfully used for the determination of the chemical environment of several transition metals [10–15,21,24–33].

2.2. X-ray absorption spectroscopy

X-ray absorption spectroscopy (XAS) is the conventional technique for analyzing the chemical environment of an element in an unknown material and was developed in the early 1970s [5]. The acronym XAS covers both X-ray absorption near edge structure (XANES) and extended X-ray absorption fine structure (EXAFS) spectroscopy techniques. XANES can be used to determine the valence state and coordination geometry, while EXAFS can be used to determine the local molecular structure, distance and coordination number of the surrounding atoms, of a particular element within a sample. A summary of this technique can be found in Refs. [34,35]. The XANES region includes the pre-edge, the edge, and the first oscillations, containing chemical and structural information of the absorber atom [36]. The edge energy for an element in a higher oxidation state is usually shifted by up to several electronvolts to a higher X-ray energy [37]. The intensity of the pre-edge peak is generally used qualitatively to obtain information on symmetry site. In the case of Mn K-edge, pre-edge properties are related to electronic transition from 1*s* core levels to the empty 3d levels, more or less 4p hybridized by the ligand, probing thus the density of the lowest unoccupied state. These electronic transitions become dipolar allowed when the inversion center is lost. In this case, the lost of symmetry permits partial overlapping and mixing of the unfilled d state of the metal with the 4p orbital of the metal. Pre-edge intensity will be virtually zero (under dipole approximation) in the case of regular O symmetry around the absorber, whereas it will have a higher intensity in the case of the T symmetry. Actually, as the main transitions at the K-edge are electric dipolar allowed, it is assumed that the pre-edge peak area could be correlated to the percentage of metal 4p atomic orbital hybridized with the metal 3d atomic orbitals [38].

3. Experimental

Determination of oxidation state and site occupancy for spinel-type oxides $Mn_{(2-x)}V_{(1+x)}O_4$ ($x=0$ and $\frac{1}{3}$) by means of high-resolution Kβ emission spectroscopy and X-ray absorption spectroscopy was performed using different simple oxides and oxyspinels of Mn and V.

3.1. Sample synthesis

The $Mn_{(2-x)}V_{(1+x)}O_4$ ($x=0$ and $\frac{1}{3}$) compounds were synthesized using MnO, V_2O_3 and VO_2 mixing them in different concentrations according to the corresponding of the desired phases. Further details of these characterizations can be found in Ref. [3]. XES and XAS manganese measurements were carried out using

standard samples of spinel-type double oxides: $Mn_{(1+z)}Cr_{(2-z)}O_4$ and $Zn_{(1-z)}Mn_{(2+z)}O_4$ ($z=0$, 0.25, 0.5, 0.75 and 1) elaborating them by traditional ceramic methods, mixing specific stoichiometric quantities of the corresponding simples oxides (see Ref. [2]). Vanadium was standardized against V_2O_3, VO_2 and V_2O_5, because V-bearing spinels are rather difficult to synthesize and the products require an independent confirmation of the oxidation state of V. Samples quality was evaluated by laboratory powder X-ray diffraction. Standard samples identity and purity were controlled by the Rietveld method using the FULLPROF software [39]; whereas formal oxidation states and site occupancy of Mn in standard spinel-type double oxides are already known [2].

3.2. XES measurements

High-resolution Kβ spectra were obtained at National Synchrotron Light Laboratory – LNLS (Campinas, Brazil) [40] and at *Facultad de Matemática, Astronomía y Física* (FAMAF), *Universidad Nacional de Córdoba*, Argentina [24]. The non-conventional spectrometer used is based on a spherically focusing crystal analyzer operated at nearly back-diffraction geometry capable to achieve high energy-resolution spectrum characterization. Both of these spectrometers were previously employed to study several Cr and Mn compounds [24,27,32]. The large effective area of the analyzer allows it to collect scattered radiation in a solid angle up to 32 msr. Symmetrical reflection geometry was used, so that excitation and further detection was measured at 45° geometry. The whole spectrometer (sample holder, analyzer and detector) is enclosed in an evacuated chamber (~0.05 mbar) avoiding X-ray attenuation and scattering from air. The incident beam flux is monitored by registering scattered radiation from a Mylar film across the incident beam path. Both main and monitor measurements were performed by a 7 mm^2 active area of Si pin diode detectors.

The spectrometer installed at FAMAF, mounted on an adapted Philips horizontal goniometer PW1380, was employed for characterization of Mn compounds. The whole spectrum from a cobalt-target X-ray conventional tube, operated at 37.5 kV and 40 mA, was used as irradiation source. High-resolution Kβ emission spectra were measured by a recorded scanning procedure consisting of 0.3 eV steps around the main line by moving the analyzer and the detector synchronously. The analyzer curvature radius is (410 ± 2) mm and the Bragg angle corresponding to the Mn-$K\beta_{1,3}$ line is 84.2° using the (440) reflection of the Si(110) spherically analyzer. An indicator of counting rates was around 950 counts s^{-1} for a spot size of 1.2 mm^2 in measurements of the $K\beta_{1,3}$ line of $Mn_{(2-x)}V_{(1+x)}O_4$ ($x=0$ and $\frac{1}{3}$) whereas the signal-to-background ratio was better than 40. The resolution of this spectrometer was determined to be 0.8 eV for the Mn $K\beta_{1,3}$ line. For calculation details see Ref. [40]. The whole acquisition time for each spectrum was 150 min, approximately.

On the other hand, when considering V compounds it was necessary to acquire high resolution spectra adapting and installing the spectrometer at the D12A-XRD1 beamline of the LNLS, because conventional X-ray source do not offer good enough total photon flux in this case. Samples were excited by a 5.57 keV monochromatic beam and the energy analysis of fluorescence photons was performed by a focusing Si(331) crystal scanning, in steps of about 0.7 eV, around the V-$K\beta_{1,3}$ emission line, whose Bragg angle is 66.46°. The calculated energy resolution was 10.5 eV for the V-$K\beta_{1,3}$ line [40]. Clearly, the obtained energy-resolution for V spectra was poorer than in the case of Mn, due to the notable difference in the analyzer Bragg angle. The curvature radius of this analyzer is (419 ± 2) mm. In the case of $Mn_{(2-x)}V_{(1+x)}O_4$ ($x=0$ and $\frac{1}{3}$) spinel-type oxides the whole acquisition time for each spectrum was around 180 min. The $K\beta_{1,3}$ line counting rate was of around 400 count s^{-1} for a spot size of 3.0 mm^2 and the signal-to-background ratio was better than 70.

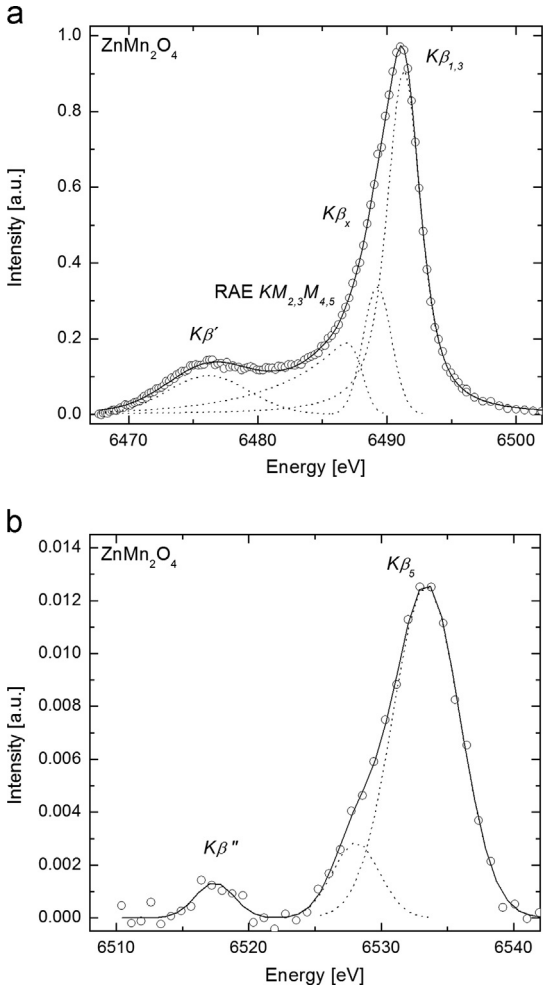

Fig. 1. Mn-Kβ emission spectrum of $ZnMn_2O_4$. (○): Experimental data. (—): Fitting curve and the corresponding contributions of individual Voigt and EMG functions (—) in the Kβ main region (a) and three Voigt functions in the Kβ″–$K\beta_5$ region (b).

The energy scale was calibrated using the value of the $K\beta_{1,3}$ line of Mn^0 and V^0 given by Bearden [41] ($EK\beta_{1,3}=6490.45$ eV for Mn and 5427.29 eV for V). The spectra were normalized to the incident intensity accounting for beam fluctuations, and a linear background was subtracted so that accurate spectral parameters might be attained. Besides, each measured spectrum were normalized to a constant value for the maximum of $K\beta_{1,3}$ line, in order to compensate differences of concentration and other conditions among different samples. Estimations of uncertainties associated with experimental procedures were determined for all spectral parameters of interest by means of fitting errors. Fig. 1 shows three Voigt functions, representing the Kβ′, $K\beta_x$ and $K\beta_{1,3}$ peaks. Additionally, Exponentially Modified Gaussian (EMG) functions, necessary to include RAE contribution, were fitted in order to reproduce the peaks features in the main Kβ region. When considering regions including the Kβ″ and $K\beta_5$ lines, in the approach of major contributions, three Voigt functions were used to fit the experimental spectra, one for Kβ″ and two for $K\beta_5$. The energy position of the RAE peak was determined from the atomic energy of the $M_{4,5}$ level [20]. Due to the low resolution in V compounds, only four Voigt function were fitted representing all the Kβ spectral features, as shown in Fig. 2.

3.3. XAS measurements

To verify the obtained results of Mn and V from high-resolution XES, Mn-K X-ray absorption spectra were performed. The experimental Mn K-edge XAS spectra were acquired at the D04B-XAFS1 beamline of the LNLS. The XAS spectra were measured using a Si (111) single channel-cut crystal as beam monochromator and a slit aperture of 0.3 mm achieving energy resolution of about 1 eV [42]. The XAS spectra were collected in transmission mode using three ion chambers, with air at atmospheric pressure, as detectors. The energy calibration was accomplished by simultaneous absorption measurements on the Mn metal sample positioned between the second and the third ionization chamber. Suitable amounts of powered compounds were deposited on a cellulose membrane to attain an optimal sample thickness for transmission experiments (edge jump close to 1). Normalized XANES spectra were obtained by the Multiplatform Applications for XAFS code (MAX) [43]. As an example, Fig. 3 reports XANES spectra corresponding to $Mn_{(2-x)}V_{(1+x)}O_4$ ($x=0$ and $\frac{1}{3}$) spinels-type double oxides. There can be appreciated typical spectrum characteristics: the pre-edge peak, the edge energy position and the first oscillations. The Mn_2VO_4 data have been move upwards 0.2 to avoid data overlapping. Due to the complexity of the spinels, achieved fittings of the EXAFS spectra were not reliable enough, therefore this part of the XAS spectra was not considered in this work.

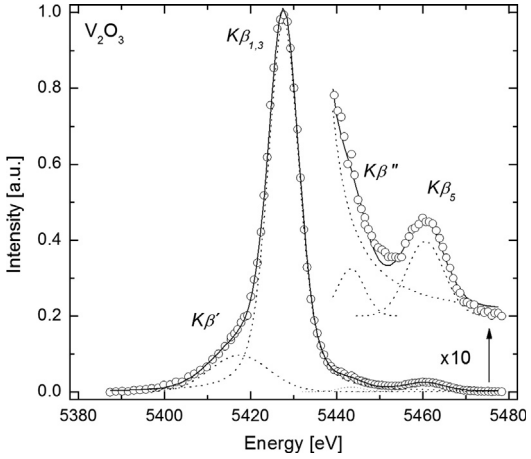

Fig. 2. V-Kβ emission spectrum of V_2O_3. (○): Experimental data. (—): Fitting curve and the corresponding contributions of individual Voigt functions (—). The Kβ″–Kβ$_5$ region was expanded in order to make clear its structure.

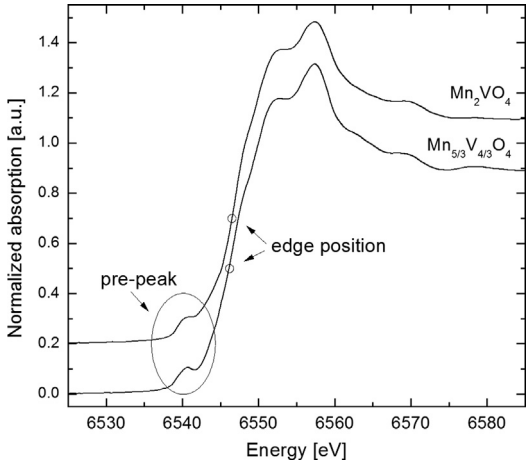

Fig. 3. Mn K-edge XANES spectra of studied spinels. The Mn_2VO_4 data has been move upwards 0.2 to avoid data overlapping.

4. Results and discussions

The chemical effects on XES are well known. Actually, they were often used to characterize of chemical bonding. Thereafter, the specific features of a high-resolution X-ray emission spectrum are related to the local structure of the studied atoms (Mn or V). Several parameters of the Kβ spectrum change with the chemical environment [10,11,13,14,24,25,27] without dependence upon relative intensity but being correlated to energy resolution. Thereby it becomes necessary attain convenient spectral parameters selections to quantify the oxidation state (coordination), looking for certain parameters varying linearly with the oxidation state (coordination) of the standard samples. In the case of Mn compounds, one of the oxidation state quantification parameter used was the intensity of contributions of RAE $KM_{2,3}M_{4,5}$ line relative to the total area of Kβ region (hereafter IRAE). The other spectral parameter was the integral of the absolute values of the difference between two spectra, one of which is considered as reference spectrum (hereafter IAD) [44]. Particulary, the $MnCr_2O_4$ spectrum was taken as the reference spectrum. The IAD parameter accounts information from the entire spectrum and it can be computed without requirements of preceding results obtained from theoretical models. It is only necessary to perfom a simple pre-analysis: area normalization and main line alignment using its first moment, which was calculated considering nothing but the spectrum region with intensities greater than 50% relative to the maximum intensity. This alignment is necessary to enhance the spectral differences in satellites lines due to changes in the chemical environment of the element under study. This parameter can be directly obtained, but requiring analog acquisition conditions for the whole set of experimental data. When using IRAE and IAD parameters, oxidation states of unknown samples were determined by the parameters of equation of the best-fit line, as shown in Figs. 4 and 5. The calculated spinels oxidation states values and corresponding uncertainties, determined by error propagation, are presented as an inset in the corresponding figures.

Fig. 4 shows relative intensities between 14% and 20% for RAE $KM_{2,3}M_{4,5}$ transition obtained by the fitting procedure. According to the theory [45], KMM line should be 1–6% of the intensity of the

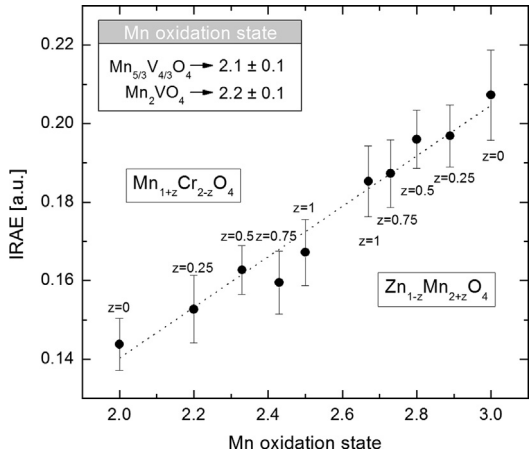

Fig. 4. Intensity of RAE $KM_{2,3}M_{4,5}$ peak relative to the total area of Kβ region as function of Mn oxidation state. (•): $Mn_{(1+z)}Cr_{(2-z)}O_4$ and $Zn_{(1-z)}Mn_{(2+z)}O_4$ ($z=0$, 0.25, 0.5, 0.75 and 1) spinel-type double oxides. (—): Linear regression of experimental data. Inset: calculated Mn oxidation state for $Mn_{(2-x)}V_{(1+x)}O_4$ spinels using the linear regression.

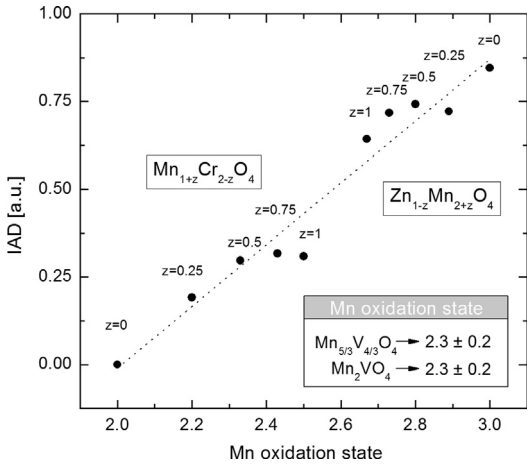

Fig. 5. IAD parameter as a function of Mn oxidation state. (•): $Mn_{(1+z)}Cr_{(2-z)}O_4$ and $Zn_{(1-z)}Mn_{(2+z)}O_4$ (z=0, 0.25, 0.5, 0.75 and 1) spinel-type double oxides. (—): Linear regression of experimental data. Error bars are smaller than the spot size. Inset: calculated Mn oxidation state for $Mn_{(2-x)}V_{(1+x)}O_4$ spinels using the linear regression.

$K\beta_{1,3}$ lines [46,47]. However, they do not distinguish between inner-shell M electrons (3s, 3p) and valence electrons. It is also known that the intensity of the RAE line in certain X-compound (where X=transition metal) is greater than for the X pure element, and also dependent on their chemical environment [19,46,48], and most of the RAE emission studies were for pure elements. In addition, this region of the spectrum also include some multiplets structure predicted by crystal-field multiplet calculations [49–51] which was not deconvolved in this work to facilitate spectral analysis. The increase in the IRAE with oxidation state, as shown in Fig. 4, can be qualitative explained, regardless the multiplet contribution [50,51], by the change in the screening effect in the 3d shell. When the oxidation state increases, the number of electrons in the 3d shell decreases then its screening effect is reduced. Then, the 3d electrons became more localized. The localized electrons are more subject to the sudden change in the atomic potential than the delocalized electrons; hence the localized electrons are more easily shaken off from the atom [19] and the probability of corresponding RAE process increases.

Regarding the IAD parameter, it resulted proportional to the nominal spin S thus being useful to the study of the spin state in a particular compound [44]. When considering Mn compounds in a high spin state, S is related to the oxidation state of manganese (O_{Mn}) by $S=7-O_{Mn}$, and IAD parameterizations trend to follow a linear relationship with a negative slope, as shown in Fig. 5. IAD uncertainties were calculated based on the IAD definition by considering statistical deviations corresponding to parameters' values smaller than the spot size. It were found slight dispersions of data suggesting that this parameter might be suitable for oxidation state quantification even considering direct calculations and minor experimental data treatment.

The $K\beta_5$ band is affected by changes of oxidation state and it has also some structures in both cases depending on the coordination number [11,24,25]. The $K\beta_5$ band is formed by transitions filling the metal 1s vacancy from orbitals contributions arising mainly from oxygen-2p and metal-3d for T symmetry, and also from ligand-2p for O symmetry. Similarly, the spinel-type oxide Mn_3O_4 ($Zn_{(1-z)}Mn_{(2+z)}O_4$, z=1) takes as well distorted spinel structure, therefore one-third of the Mn has a coordination number four (site A) and two-thirds have six (site B). When considering the case of spinel-type oxide $Mn_{(1+z)}Cr_{(2-z)}O_4$ with z=0, it has a Mn^{2+} ion, occupying site A, with coordination number four; when the Mn/Cr ratio is more than $\frac{1}{2}$ excess Mn ions replace chromium ions in site B as Mn^{3+}. Unlike, $Zn_{(1-z)}Mn_{(2+z)}O_4$ with z=0 is also a normal spinel and Mn^{3+} occupies site B, then their coordination number is six and when the Mn/Zn ratio is greater than 2, excess Mn ions replace Zn ions in site A as Mn^{2+}. For the whole series of spinel-type oxide $Zn_{(1-z)}Mn_{(2+z)}O_4$ and $Mn_{(1+z)}Cr_{(2-z)}O_4$ (z=0, 0.25, 0.5, 0.75 and 1), the coordination number of Mn can be assessed by relatively simple relationships [2].

Fig. 6 shows the $K\beta_5$ intensity relative to the total intensity of Kβ region ($IK\beta_5$) as a function of Mn coordination number for the studied spinel-type oxide series. It can be observed an increasing linear tendency with a clear dispersion of calculated values, being the $IK\beta_5$ uncertainties greater than previous cases (see Figs. 4 and 5). An increase in coordination number enlarges valence-to-core transition probabilities, involving the atomic orbital 2p of the ligand representing the main contribution in the $K\beta_5$ peak. Thereby, global growing tendencies of the $IK\beta_5$ parameter with the Mn coordination might be explained showing also good agreement with Eba and Sakurai [2]. In order to characterize the Mn coordination in the studied spinels, a linear regression to corresponding values of spinel-type oxide were fitted to determine the Mn coordination numbers of samples being studied. The obtained results for Mn coordination numbers mean values and corresponding uncertainties are presented in Fig. 6.

The poor energy resolution achieved for V spectra measurements (about 11 eV) precluded separation of the RAE $KM_{2,3}M_{4,5}$ line and multiples structure contributions from that of the $K\beta_{1,3}$ line, and that the spectral differences of V-compounds with different oxidation state were very slight. So, poor energy resolution limited V compounds characterization avoiding the use of the same parameters as for Mn compounds. Instead, the intensity of the line Kβ′ relative to the total area of Kβ region ($IK\beta'$) was used. Fig. 7 shows the inverse linear relationship of $IK\beta'$ with the oxidation state for V simple oxides. The Kβ′ intensity, according to Tsutsumi's model [52], should be quite proportional to the ratio between final state multiplicities, leading to $S/(S+1)$, S being the nominal spin in the incomplete 3d shell. Moreover, it is related to the oxidation state of vanadium (O_V) as $S=7-O_V$. According to this reasoning, and neglecting the contributions of RAE $KM_{2,3}M_{4,5}$ and $K\beta_x$ lines, simple models might satisfactory describe the decreasing trend of $IK\beta'$ with O_V, but on the other hand it might fail to accurately reproduce its functional dependence [27]. The oxidation state of V in the unknown samples was determined using the calibration line of V_2O_3, VO_2 and V_2O_5 data, as shown in Fig. 7. Simple V oxides were used to determine the oxidation state of V in

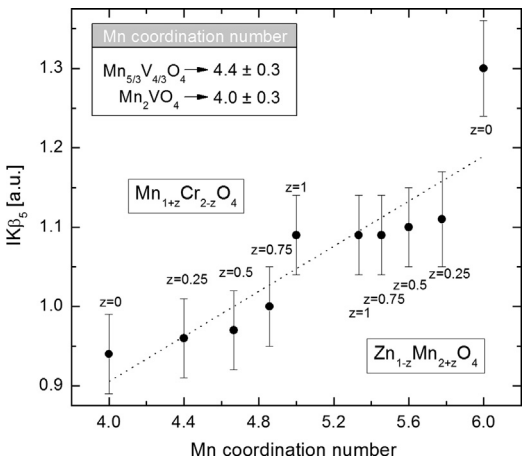

Fig. 6. $K\beta_5$ intensity relative to the total area of Kβ region as function of Mn coordination number. (•): $Mn_{(1+z)}Cr_{(2-z)}O_4$ and $Zn_{(1-z)}Mn_{(2+z)}O_4$ (z=0, 0.25, 0.5, 0.75 and 1) spinel-type double oxides. (—): Linear regression of experimental data. Inset: calculated Mn coordination number for $Mn_{(2-x)}V_{(1+x)}O_4$ spinels using the linear regression.

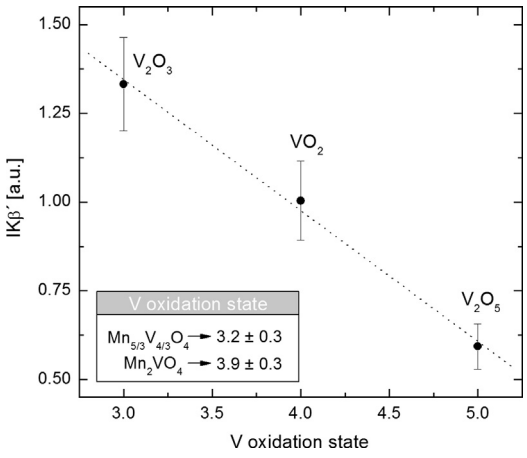

Fig. 7. Kβ′ intensity relative to the total area of Kβ region as function of V oxidation state for simple oxides (•). (—): Linear regression of experimental data. Inset: calculated V oxidation state for $Mn_{(2-x)}V_{(1+x)}O_4$ spinels using the linear regression.

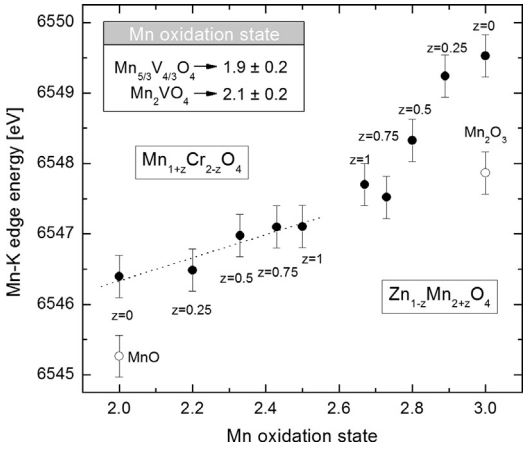

Fig. 8. Mn-K absorption edge energy as function of Mn oxidation state. (○): Mn simple oxides. (•): $Mn_{(1+z)}Cr_{(2-z)}O_4$ and $Zn_{(1-z)}Mn_{(2+z)}O_4$ ($z=0$, 0.25, 0.5, 0.75 and 1) spinel-type double oxides. (—): Linear regression corresponding to $Mn_{(1+z)}Cr_{(2-z)}O_4$ experimental data. Inset: calculated Mn oxidation state for $Mn_{(2-x)}V_{(1+x)}O_4$ spinels using the linear regression.

the studied samples because V-bearing spinels are rather difficult to synthesize and the products require an independent confirmation of the oxidation state of V. The sum of cations charges, taking into account the calculated V and Mn oxidation states, gives consistent and appropriate results (c.a. 8, the absolute value of anions charge).

In order to compare the Mn and V characterization results of the spinel-type oxides $Mn_{(2-x)}V_{(1+x)}O_4$ ($x=0$ and $\frac{1}{3}$) by high-resolution Kβ XES, Mn-K XANES spectra were used to determine the oxidation state and the coordination, using the edge energy position and pre-edge area, respectively. From the X-ray absorption spectrum, energy position was measured determining the edge energy half way up the normalized-edge step as usual for absorption equal to 0.5. Clearly, two different linear tendencies are observed in Fig. 8, corresponding to each standard sample group (Cr-bearing spinels and Zn-bearing spinels). When considering oxidation states 2+ and 3+, significant dispersions were found for Mn-K edge energy between spinel-type oxides and simple oxides, reinforcing the fact that the edge energy not only depends on the oxidation state but also on the chemical environment [36]. Then, the Cr-bearing spinel linear fit was used for Mn oxidation state determination in the $Mn_{(2-x)}V_{(1+x)}O_4$ spinels, since their Mn-K edge energies are similar. The obtained values of Mn oxidation states in $Mn_{(2-x)}V_{(1+x)}O_4$ ($x=0$ and $\frac{1}{3}$) spinels exhibit good agreement with those corresponding to XES techniques, as shown as insets show in the reported figures.

To extract the pre-edge feature, the contribution of the edge jump to the pre-edge was modeled near pre-edge with a Lorentzian function. The area of the extracted pre-edge, calculated by a simple integral, as a function of Mn coordination number is shown in Fig. 9 for the series of spinel-type oxide $Zn_{(1-z)}Mn_{(2+z)}O_4$ and $Mn_{(1+z)}Cr_{(2-z)}O_4$ ($z=0$, 0.25, 0.5, 0.75 and 1). It was found a remarkable linear behavior with slight dispersions. It has to be highlighted that the two spinel-type oxide series show the same linear behavior, unlike what is observed in Fig. 8. The symmetry around absorbing atom strongly affects pre-edge transition, finding a very low intensity pre-edge peak for O symmetry and largest for pure T symmetry [53,54]. Increasing z (from 0 up to 1) in $Zn_{(1-z)}Mn_{(2+z)}O_4$ diminishes the Mn occupancy of site B (related to the O symmetry), and decreasing z (from 1 up to 0) in $Mn_{(1+z)}Cr_{(2-z)}O_4$ the Mn occupancy of site B decreases too. The $MnCr_2O_4$ spinel has a pure T symmetry showing the greatest value of pre-edge area, while $ZnMn_2O_4$, with an O distorted symmetry by Jahn–Teller effect, exhibits the lowest value [54]. A linear regression to corresponding values of spinel-type oxide series was fitted to determine the unknown coordination of the studied samples. The obtained results are shown in Fig. 9. The calculated Mn coordination number of $Mn_{5/3}V_{4/3}O_4$ agrees with those determined using IKβ$_5$ parameter. Unlike, in the case of Mn_2VO_4 the Mn coordination values are significantly different, thus suggesting that more reliable the coordination number obtained by means of Mn-K pre-edge area perhaps due to possible mixed effects (chemical and atomic) in the Kβ$_5$ band [11]. Besides, the Mn coordination numbers obtained for $Mn_{(2-x)}V_{(1+x)}O_4$ ($x=0$ and $\frac{1}{3}$) spinels, using pre-edge area reported in Fig. 9 are in good agreement with the Mn site occupancies obtained by Pannunzio-Miner et al. [3].

The oxidation state and coordination number of cations in the $Mn_{(2-x)}V_{(1+x)}O_4$ ($x=0$ and $\frac{1}{3}$) spinels, determined by high-resolution XES and XANES spectra are presented in the insets of Figs. 4–9. The Mn oxidation state values, calculated according to the parameters described above and based on both emission and absorption spectra, were indistinguishable and equal to 2+. This issue suggests to fortify the model regarding the oxidation states of Mn and the site occupancies in $Mn_{(2-x)}V_{(1+x)}O_4$ ($x=0$ and $\frac{1}{3}$) spinels assumed, without precise experimental descriptions by Pannunzio-Miner et al. [3]. Then, if the oxidation state of V is fixed by charge-balance constraints it implies 4+ for Mn_2VO_4 and 3.5+ for $Mn_{5/3}V_{4/3}O_4$, being in good agreement with the calculated values.

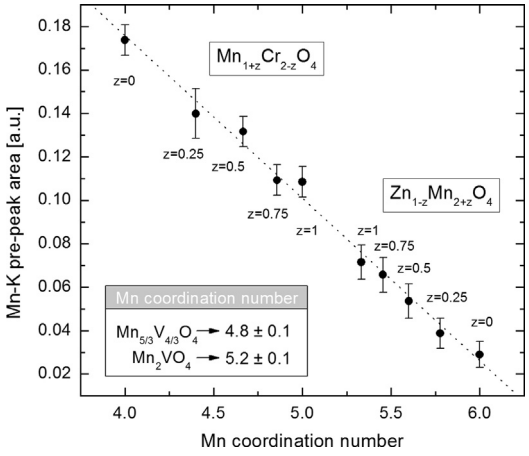

Fig. 9. Mn-K absorption pre-peak area as function of Mn coordination number. (•): $Mn_{(1+z)}Cr_{(2-z)}O_4$ and $Zn_{(1-z)}Mn_{(2+z)}O_4$ ($z=0$, 0.25, 0.5, 0.75 and 1) spinel-type double oxides. (—): Linear regression of experimental data. Inset: calculated Mn coordination number for $Mn_{(2-x)}V_{(1+x)}O_4$ spinels using the linear regression.

It should be stressed that no oxygen vacancies were detected in these spinels [3], so that a total negative charge of 8 can be safely assumed. It can be also observed that the calculated oxidation state through IRAE parameter have relative confidence deviations of 5% being lower than relative uncertainties for other parameters. It might be associated to small dispersion of the experimental data. On the other hand, the obtained results for the IAD parameter exhibit relative deviations of 9%. But when considering oxidation states between 2+ and 3+, the IAD parameter presents larger variations than the other parameters, which might be interpreted as high sensitivity to distinguish oxidation states. Although oxidation state determination of V in the studied samples was performed using V simple oxides, the obtained results showed a good behavior with relative deviations of 9%.

Regarding the characterization of coordination by XANES spectra, it is to point out that results obtained using the Mn-K pre-edge area show good performance presenting relative deviations of 2%. Hence, it constitutes evidence for supporting that this seems to be suitable in order to assess the coordination number of an atom. Despite presenting relative deviations of about 8%, results for coordination number achieved with the IKβ_5 parameter do not appear in correspondence with the expected appropriate behavior, getting an indistinguishable (distinguishable) results for the sample $Mn_{5/3}V_{4/3}O_4$ (Mn_2VO_4) calculating the corresponding coordination number by Mn-K pre-edge area and neutrons diffraction: 4.8 and 5.1 for $Mn_{5/3}V_{4/3}O_4$ and Mn_2VO_4, respectively [3]. Some reasons to discrepancies might be due to oversimplifications for the origin of the Kβ_5, which was assumed as a cross-over transition. It is known by molecular orbitals calculations that this line is not a pure cross-over transition but also has quadrupolar contributions which reduced its dependence with coordination [52].

5. Conclusions

X-ray emission spectroscopy is a useful technique to determine oxidation states of transition elements in complex compounds like spinels. This technique is based on the analysis of satellite lines in emission spectra arising from transitions between valence orbitals and the metal ion 1s level. High-resolution Kβ spectra provide information that is complementary to other spectroscopic techniques, like XANES and EXAFS. Although absorption techniques, like XANES, are well established, the possibility of using XES with conventional X-ray sources (as opposed to synchrotron-generated radiation) makes it a versatile and low-cost technique. The obtained data were useful for obtaining first chemical environmental characterization of spinel-type oxides family, and confirm the model regarding the oxidation states of V and Mn and their site occupancies in $Mn_{(2-x)}V_{(1+x)}O_4$ spinels proposed by Pannunzio-Miner et al. [3]. Hence, the developed method demonstrated to be capable of assess magnetic and transport properties in this spinel-type oxides, constituting a valuable tool for technical applications.

A detailed study of high resolution Kβ X-ray emission spectra of family members spinel $Mn_{(2-x)}V_{(1+x)}O_4$ ($x=0$ and $\frac{1}{3}$) was performed to get the oxidation states and coordination of Mn and V. The obtained results were verified with X-ray absorption spectra, showing a very good concordance in the oxidation state determination. The intensity of RAE $KM_{2,3}M_{4,5}$ relative to the total area intensity along with IAD values were used as reference parameters to Mn oxidation state characterizations. Furthermore, it proved to be a useful parameter when considering spectrum measurements with high energy resolution. While IRAE proved a good parameter to oxidation state characterization, it is necessary to note that the spectral region containing this contribution is also affected by a broad multiplet structure. In addition, there may be also contributions of X-ray Raman scattering [49–51]. Therefore, it is clear that a detailed and thorough study, both theoretical and experimental, is needed to determine separately the contributions of mutiplets and RAE in this region of the spectrum, and its dependence on the oxidation state. In the cases of V compounds, it was used the intensity of the line Kβ′ relative to the total area. Parameters' uncertainties calculated by XES characterizations were similar to that obtained by XAS.

In addition, the coordination number of Mn was found using the Kβ spectra but some discrepancies with XAS determination were found. As mentioned, this feature might be due because this band is not a pure cross-over transition actually having quadrupolar contributions weakening its dependence with coordination number [52]. A deeply study of Kβ_5 band behavior may be necessary, especially for complex compounds, to elucidate its dependence with coordination, allowing to be considered to coordination characterization.

Acknowledgments

The research was supported by LNLS, Brazilian Synchrotron Light Laboratory (Projects D12A-XRD1-9294 and 9843). Financial supports from the *Consejo Nacional de Investigaciones Científicas y Técnicas* (CONICET) and from the *Secretaría de Ciencia y Técnica de la Universidad Nacional de Córdoba* (UNC) are gratefully acknowledged. The authors thank S. Limandri for helpful comments. The authors also thank C. Cusatis and LORXI – *Laboratório de Óptica de Raios X e Instrumentação*, *Universidade Federal do Paraná*, for useful discussions and technical assistance.

References

[1] B.E. Martin, A. Petric, J. Phys. Chem. Solids 68 (2007) 2262–2270.
[2] H. Eba, K. Sakurai, J. Solid State Chem. 178 (2005) 370–375.
[3] E.V. Pannunzio-Miner, J.M. De Paoli, R.D. Sánchez, R.E. Carbonio, Mater. Res. Bull. 44 (2009) 1586–1591.
[4] A.P. Ramirez, R.J. Cava, J. Krajewski, Nature 386 (1997) 156–159.
[5] D.E. Sayers, E.A. Stern, F.W. Lytle, Phys. Rev. Lett. 27 (1971) 1204–1207.
[6] I. Levin, V. Krayzman, J.C. Woicik, A. Tkach, P.M. Vilarinho, Appl. Phys. Lett. 96 (2010) 052904.
[7] A. Yang, Z. Chen, A.L. Geiler, X. Zuo, D. Haskel, E. Kravtsov, C. Vittoria, V.G. Harris, Appl. Phys. Lett. 93 (2008) 052504.
[8] A. Okita, F. Saito, S. Sasaki, T. Toyoda, H. Koinuma, Jpn. J. Appl. Phys. 37 (1998) 3441–3445.
[9] P. Glatzel, U. Bergmann, Coord. Chem. Rev. 249 (2005) 65–95.
[10] M.A. Beckwith, M. Roemelt, M. Collomb, C. DuBoc, T. Weng, U. Bergmann, P. Glatzel, F. Neese, S. DeBeer, Inorg. Chem. 50 (2011) 8397–8409.
[11] E. Gallo, F. Bonino, J.C. Swarbrick, T. Petrenko, A. Piovano, S. Bordiga, D. Gianolio, E. Groppo, F. Neese, C. Lamberti, P. Glatzel, Chem. Phys. Chem. 14 (2013) 79–83.
[12] M.U. Delgado-Jaime, B.R. Dible, K.P. Chiang, W.W. Brennessel, U. Bergmann, P.L. Holland, S. DeBeer, Inorg. Chem. 50 (2011) 10709–10717.
[13] S.G. Eeckhout, O.V. Safonova, G. Smolentsev, M. Biasioli, V.A. Safonov, L.N. Vykhodtseva, M. Sikoraa, P. Glatzel, J. Anal. At. Spectrom. 24 (2009) 215–223.
[14] K.M. Lancaster, Y. Hu, U. Bergmann, M.W. Ribbe, S. DeBeer, J. Am. Chem. Soc. 135 (2013) 610–612.
[15] K.M. Lancaster, K.D. Finkelstein, S. DeBeer, Inorg. Chem. 50 (2011) 6767–6774.
[16] G. Peng, F.M.F. deGroot, K. Hämäläinen, J.A. Moore, X. Wang, M.M. Grush, J.B. Hastings, D.P. Siddons, W.H. Armstrong, O.C. Mullins, S.P. Cramer, J. Am. Chem. Soc. 116 (1994) 2914–2920.
[17] E. Cengiz, Z. Bıyıklıoğlu, N. Küp Aylıkcı, V. Aylıkcı, G. Apaydın, E. Tıraşoğlu, H. Kantekin, Chin. J. Chem. Phys. 23 (2010) 138–144.
[18] S.P. Limandri, A.C. Carreras, R.D. Bonetto, J.C. Trincavelli, Phys. Rev. A: At., Mol., Opt. Phys. 81 (2010) 012504.
[19] J. Kawai, T. Nakagima, T. Inoue, H. Adachi, M. Yamaguchi, K. Maeda, S. Yabuki, Analyst 119 (1994) 601–603.
[20] J.A. Bearden, A.F. Burr, Rev. Mod. Phys. 39 (1967) 125–142.
[21] N. Lee, T. Petrenko, U. Bergmann, F. Neese, S. DeBeer, J. Am. Chem. Soc. 132 (2010) 9715–9727.
[22] C.J. Pollock, S. DeBeer, J. Am. Chem. Soc. 133 (2011) 5594–5601.
[23] H. Adachi, S. Shiokawa, M. Tsukada, C. Satoko, S. Sugano, J. Phys. Soc. Jpn. 47 (1979) 1528–1537.
[24] G. Tirao, S. Ceppi, A.L. Cappelletti, E.V.Pannunzio Miner, J. Phys. Chem. Solids 71 (2010) 199–205.

[25] U. Bergmann, C.R. Horne, T.J. Collins, J.M. Workman, S.P. Cramer, Chem. Phys. Lett. 302 (1999) 119–124.
[26] U. Bergmann, P. Glatzel., Photosynth. Res. 102 (2009) 255266.
[27] S. Limandri, S. Ceppi, G. Tirao, G. Stutz, C.G. Sánchez, J.A. Riveros., Chem. Phys. 367 (2010) 93–98.
[28] S.D. Gamblin, D.S. Urch, J. Electron. Spectrosc. Relat. Phenom. 113 (2001) 179–192.
[29] W. Hua, K. Zhou, Y. Huang, Q. Qian, W. He, S. Ma, W. Chu, T. Hu, Z. Wu, Spectrochim. Acta, Part A 70 (2008) 462–465.
[30] Q. Qian, T.A. Tyson, C.-C. Kao, J.-P. Rueff, F.M.F. de Groot, M. Croft, S.-W. Cheong, M. Greenblatt, M.A. Subramanian, J. Phys. Chem. Solids 61 (2000) 457–460.
[31] C. Suzuki, J. Kawai, H. Adachi, T. Mukoyama, Chem. Phys. 247 (1999) 453–470.
[32] M. Torres Deluigi, G. Tirao, G. Stutz, C. Cusatis, J.A. Riveros, Chem. Phys. 325 (2006) 477–484.
[33] N. Lee, T. Petrenko, U. Bergmann, F. Neese, S. DeBeer, J. Am. Chem. Soc. 132 (2010) 9715–9727.
[34] J. Kawai, in: R.A. Meyers (Ed.), Encyclopedia of Analytical Chemistry, John Wiley & Sons Ltd., Chichester, 2000, pp. 13288–13315.
[35] F. deGroot, Chem. Rev. 101 (2001) 1779–1808.
[36] P. Chaurand, J. Rose, V. Briois, M. Salome, O. Proux, V. Nassif, L. Olivi, J. Susini, J.L. Hazemann, J.Y. Bottero, J. Phys. Chem. B 111 (2007) 5101–5110.
[37] S.D. Kelly, D. Hesterberg, B. Ravel, in: A.L. Ulery, L.R. Drees (Eds.), Methods of Soil Analysis, Part 5 – Mineralogical Methods, Soil Science Society of America, Madison, 2008, pp. 387–464.
[38] J.J. Rehr, R.C. Albers, Rev. Mod. Phys. 72 (2000) 621–654.
[39] J. Rodriguez-Carbajal, Physica B 192 (1993) 55–59.
[40] G. Tirao, G. Stutz, C. Cusatis, J. Synchrotron Radiat. 11 (2004) 335–342.
[41] J.A. Bearden, Rev. Mod. Phys. 39 (1967) 78–124.
[42] H.C.N. Tolentino, A.Y. Ramos, M.C.M. Alves, R.A. Barrea, E. Tamura, J.C. Cezar, N. Watanabe, J. Synchrotron Rad. 8 (2001) 1040–1046.
[43] A. Michalowicz, J. Moscovici, D. Muller-Bouvet, K. Provost, J. Phys.: Conf. Ser. 190 (2009) 012034.
[44] G. Vankó, T. Neisius, G. Molnár, F. Renz, S. Kárpáti, A. Shukla, F.M.F. de Groot, J. Phys. Chem. B 110 (2006) 11647–11653.
[45] J.H. Scofield, Phys. Rev. 179 (1969) 9–16.
[46] H.R. Verma, J. Phys. B 33 (2000) 3407–3415.
[47] J.L. Campbell, A. Perujo, W.J. Teesdale, B.M. Millman, Phys. Rev. A 33 (1986) 2410–2417.
[48] S.S. Raju, B.S. Reddy, M.V.R. Murti, L. Mombasawala, X-Ray Spectrom. 36 (2007) 35–40.
[49] P. Glatzel, U. Bergmann, F.M.F. de Groot, S.P. Cramer, Phys. Rev. B 64 (2001) 045109.
[50] N.K Aylikci, E. Tirașoğlu, İ.H. Karahan, V. Aylikci, E. Cengiz, G. Apaydin, Chem. Phys. Lett. 484 (2010) 368–373.
[51] W. Cao, M. Kavčič, J.-Cl. Dousse, M. Berset, K. Bučar, M. Budnar, K. Fennane, J. Hoszowska, Y.-P. Maillard, J. Szlachetko, M. Szlachetko, M. Žitnik, Phys. Rev. A: At., Mol., Opt. Phys. 83 (2011) 042513.
[52] K. Tsutsumi, H. Nakamori, K. Ichikawa, Phys. Rev. B: Condens. Matter Mater. Phys. 13 (1976) 929–933.
[53] F. de Groot, G. Vankó, P. Glatzel, J. Phys.: Condens. Matter 21 (2009) 104207.
[54] T. Yamamoto, X-Ray Spectrom. 37 (2008) 572–584.